Available online at www.sciencedirect.com
SCIENCE DIRECT®
Journal of Solid State Chemistry 177 (2004) 575–579
JOURNAL OF SOLID STATE CHEMISTRY
http://elsevier.com/locate/jssc

Some properties of single-crystal boron carbide

H. Werheit,[a,*] A. Leithe-Jasper,[b,1] T. Tanaka,[b] H.W. Rotter,[c] and K.A. Schwetz[d]

[a] *Solid State Physics Laboratory, Experimental Physics, Gerhard Mercator University, Bensberger Marktweg 328, D-51069 Cologne, Germany*
[b] *National Institute for Materials Science, Advanced Materials Laboratory, Namiki 1-1, Tsukuba, Ibaraki 305-0044, Japan*
[c] *Institute of Inorganic and Analytical Chemistry, University of Freiburg, D-79104 Freiburg, Germany*
[d] *Wacker Ceramics, D-87437 Kempten, Germany*

Received 14 June 2002; received in revised form 22 April 2003; accepted 29 April 2003

Abstract

Large and high-quality floating zone grown single crystals of boron carbide of the composition $B_{\sim 4.3}C$ corresponding to the carbon-rich limit $B_{4.3}C$ of the homogeneity range, were presented by Leithe-Jasper and Tanaka at the ISBB'99 in Dinard for the first time. Such crystals now allow determining the physical properties of this refractory semiconductor free from the influence of impurities or coarse structural imperfections. Some solid-state properties of these single crystals like electronic transport properties, IR optical absorption spectrum, IR reflectivity spectrum, FT-Raman spectrum, and Knoop hardness are presented and discussed with respect to the properties of less perfect boron carbide previously determined. Outstanding properties are the hardness exceeding that of technical boron carbide by 14% ($\parallel c$) and 24% ($\perp c$) respectively, and the high optical absorption at energies below the absorption edge and the reflectivity strongly increasing towards low frequencies suggesting a destinctly higher contribution of free carriers.

Keywords: Boron carbide; Electronic transitions; IR spectrum; Raman spectrum; Electronic transport; Hardness

1. Introduction

The homogeneity range of the refractory semiconductor boron carbide extends from $B_{4.3}C$ at the carbon-rich to $B_{\sim 11}C$ at the boron-rich limit (see Ref. [1] and references therein). Deviations of real compounds from the hypothetically ideal $B_{13}C_2$ (structure formula, $(B_{12})CBC$) are characterized by structural defects ($B_{11}C$ icosahedra, CBB or CCC chains, B□B arrangements) in certain concentrations, which are inevitable because of the structural necessity to compensate the valence electron deficiency of the actual compound [2–4].

Most of the experimental investigations on boron carbide, which have hitherto been reported (see Ref. [1], and references therein), were performed on polycrystalline material obtained by melting or hot pressing. Few exceptions were small single crystals grown by chance during the technical production process or by metal solution growth experiments, but they usually exhibit twins in considerable concentrations. Accordingly, in no case influences of impurities, grain boundaries or coarse structural imperfections additional to those structural defects, which are intrinsic because of their correlation with the electronic properties [2,3], on the results can be definitely excluded. The preparation of big size single crystals of $B_{\sim 4.3}C$ boron carbide [5], whose composition is close to the carbon-rich limit of the homogeneity range, now allows to largely exclude the influence of grain boundaries, other coarse defects and impurities. Some experimental results obtained on such single crystals are presented below.

2. Crystal preparation

Stable floating zone crystal growth of big boron carbide single crystals ($\ominus \sim 7$ mm; $l \sim 60$ mm) was found to occur very close to the carbon-rich limit $B_{4.3}C$ of the large homogeneity range only [5]. Early attempts to grow "B_4C" crystals by the floating zone method

*Corresponding author. Fax: +49-221-682796.
E-mail address: h.werheit@uni-duisburg.de, helmut.werheit@koeln.de (H. Werheit).
[1] Present address: MPI-CPfS, Nöthnitzerstr. 40, D-01187 Dresden, Germany.

0022-4596/$ - see front matter © 2003 Elsevier Inc. All rights reserved.
doi:10.1016/j.jssc.2003.04.005

applying MHz RF-heating were made by Falckenberg [6]. Since the high melting point and corrosiveness of boron-rich melts exclude the use of crucibles, the floating zone technique was chosen to grow crystals. Below, results obtained on pieces cut from one of a series of boron carbide crystals are presented. The experimental route towards single crystals consists of two parts as detailed below.

2.1. Preparation of polycrystalline feed rods

Cylindrical ceramic green bodies ($\ominus \sim 10$ mm; $l \sim 100$ mm) were synthesized from commercially available boron carbide powder (“B_4C”, Kojundokagaku Co. Jp., purity >99 wt%; metal impurities in wt% are Si = 0.035, Fe = 0.01, Al = 0.003, Cu = 0.004, Ca = 0.002, Mg = 0.001, Mn = 0.001, Na = 0.001; grain size ~ 10 μm), containing camphor as lubricant, by isostatic pressing at about 250 MPa in rubber pipes of appropriate diameters. The composition $B_{4.38(5)}C$ of the powder was checked by a carbon analysis using the combustion method in a LECO carbon analyzer. The so formed cylindrical bodies were placed in a graphite crucible and subjected to a heat treatment program in a conventional RF-heating furnace under vacuum of about 3×10^{-8} Pa. Slow heating to a level at a moderate temperature enables smooth evaporation of the camphor binder. Subsequent heating to $T > 2100$°C and maintaining this temperature for several hours enhances the grain growth and thus favors dense sintering. Successful crystal growth can be accomplished with dense sintered feed rods only. Otherwise, the melt immediately permeates into a poorly sintered porous body making crystal growth impossible.

2.2. Floating zone crystal growth

For the refractory boron carbide, the use of a Xe high-pressure arc-discharge lamp image furnace (NEC Co., Jp.) was found to be the best way to overcome the poor coupling of this material to conventional kHz RF-heating systems at low temperatures, and the problems of indirect W-ring heating (where the melting is performed by radiation heating of the sample which passes through an inductively heated tungsten ring [7–9]) at the high melting point of boron carbide as well. The polycrystalline feed rod and the growing crystal were synchronously moved downward with 12 mm/h and counter rotated at 50 rpm in streaming pure Ar gas. The crystal obtained was characterized by X-ray powder diffraction ($a = 5.6060(14)$, $c = 12.0851(78)$ Å) and metallography. The cut and polished specimens were subject to light microscopic investigations. For the material used in this study, no indications of polysynthetic twinning commonly observed for boron carbide [6,10,11] could be found by inspecting etched samples under polarized light. The crystal was oriented by Laue back scattering techniques and cut parallel and perpendicular to [00.1] by spark erosion. X-ray (Cu$K\alpha$) rocking curves were taken for the (00.3) plane and showed a FWHM of around 100 arcsec.

The chemical composition of the single crystals was determined in two different laboratories, NIRIM and Wacker. The results are $B_{4.36(8)}C$ and $B_{4.24(10)}C$, respectively. The overlap of both results well agrees with the carbon-rich limit of the homogeneity range $B_{4.3}C$. The impurities in ppm are O (1100), N (100), Fe (100), Mg (5), Al(20), Ca (20), Si(220), and Ti (30).

3. Transport properties

In Table 1, some electronic transport properties of the $B_{\sim 4.3}C$ single crystals are compared with data on boron carbide of comparable composition ($B_{4.3}C$, “B_4C”) taken from literature (see Refs. [1,22] and references therein).

The electrical conductivity is smaller than that reported for boron carbide single crystals originating from technical production, but the Seebeck coefficent is higher. This seems to indicate that the carrier mobility increases with increasing structural quality of boron carbide.

4. Optical absorption

4.1. Range of electronic transitions

The optical absorption of boron carbide in the range of electronic transitions is very high. Results obtained on a 70 μm thick self-supporting sample of technical boron carbide were reported in Ref. [12]. Attempts to calculate the absorption spectra in this range by the Kramers–Kronig transformation of reflectivity spectra [13] failed for principle reasons because of the missing frequency-independent high-frequency dielectric constant, which is required for this calculation. Accordingly, transmission measurements for reliable absorption data require very thin samples that were

Table 1
Electronic transport properties of $B_{\sim 4.3}C$ measured at 300 K compared with data taken from Refs. [1,22]

		This work	Refs [1,22]
σ ($\parallel$c)	(Ω^{-1} cm^{-1})	0.11	8×10^{-2}–10
σ ($\perp$c)	(Ω^{-1} cm^{-1})	0.05	3×10^{-1}–5
σ	(Ω^{-1} cm^{-1})	—	5–30
S ($\parallel$c)	(μV K^{-1})	160	130
S ($\perp$c)	(μV K^{-1})	160	80
S	(μV K^{-1})	—	20–300

difficult to prepare from brittle coarse-grained material. If those are adhered to a transparent support, the results may be influenced by the absorption of the glue, and by the reflectivity losses at the support surfaces [14]. Results on the temperature-dependent absorption edge measured on a self-supporting sample of very dense hot-pressed boron carbide were presented in Ref. [14].

The preparation of a sufficiently thin sample of $B_{\sim 4.3}C$ monocrystalline boron carbide turned out to be rather difficult, because the absorption is distinctly higher than that of technical boron carbide. Finally, we succeeded in preparing a 17 μm thick self-supporting sample for the orientation $E \perp c$. Its absorption spectrum measured with a Perkin-Elmer double-grating spectrometer (Lambda 19) is displayed in Fig. 1.

The decomposition of the absorption edge according to the theories of electronic transitions yielded the following transition energies:

$E(1)$ 0.76(1) eV nondirect transition,

$E(2)$ 0.93(1) eV nondirect transition.

These transition energies well agree with two of those obtained on polycrystalline boron carbide [14]. The energy dependence of the absorption coefficient for nondirect transitions (transition between a localized level in the band gap and a band) is the same as that theoretically expected for indirect interband transitions as well. The attribution to nondirect transitions follows the argumentation and the preliminary band scheme of boron carbide presented in Refs. [1,3,15].

There is a distinct absorption band at 0.73(1) eV. To check, whether there are further absorption processes, the absorption below the edge was fitted by a third-order polynom to get a smooth reference. The difference is displayed in Fig. 2. Absorption bands at (i) 0.59 eV, (ii) 0.65 eV, (iii) 0.68 eV, and (iv) 0.73 eV are seen. Two of them, (i) and (iv), can be easily attributed to electronic transitions between localized levels above the valence band edge in the preliminary band scheme of boron

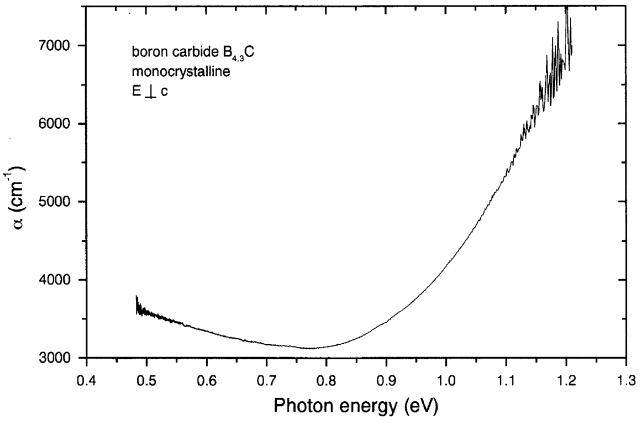

Fig. 1. Absorption coefficient vs. photon energy.

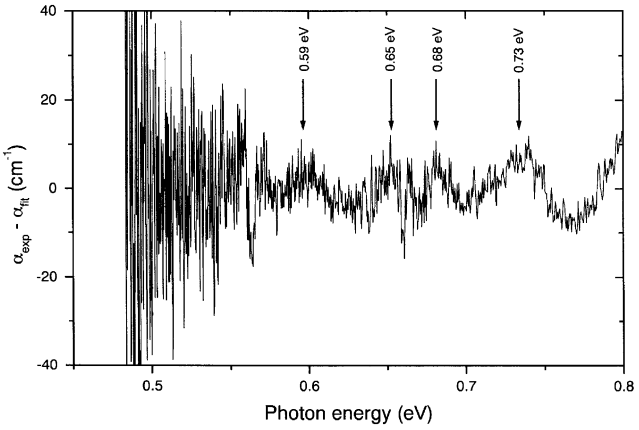

Fig. 2. Difference between the measured absorption coefficient and an empirical third-order polynom used for fitting.

carbide [1,15]: 1.20–0.47 = 0.73 eV, 0.92–0.18 = 0.74 eV and 0.77–0.18 = 0.59 eV respectively; (iii) is satisfactorily close to the difference 0.77–0.065 = 0.705 eV, if the uncertainty 0.1 eV of the measured data is considered.

The comparison of the absorption coefficients in the low-absorption range below the absorption edge (technical boron carbide, $\alpha \sim 400\,cm^{-1}$ [12]; hot-pressed dense $B_{4.3}C$, $\alpha \sim 1300\,cm^{-1}$ [14]; high-quality $B_{\sim 4.3}C$ single crystal, $\alpha \sim 3100\,cm^{-1}$ (this work)) seems to indicate that this absorption increases with increasing structural perfection. Since increasing towards lower energies, this absorption can be attributed to the absorption of charge carriers, which usually increases with decreasing imperfections of the solid. In Ref. [16], it was proved that the electronic transport in boron carbide is a superposition of hopping-type and Drude-type transport. For both electronic transport mechanisms, the absorption corresponds to the spectral dependence found in the $B_{\sim 4.3}C$ single crystal.

4.2. IR-reflectivity spectrum

The reflectivity spectrum (Fig. 3) was measured with a Bruker FTIR spectrometer. An accordingly obtained spectrum of polycrystalline $B_{4.3}C$ [16] is included for comparison. As shown in Ref. [16], the dynamical conductivity of hopping- or Drude-type transport is related to a reflectivity increase towards lower frequencies. Compared with polycrystalline $B_{4.3}C$, for the single crystal this increase is much stronger, and distinctly remarkable already in the MIR range. This strongly supports the assumption that the electrical conductivity of boron carbide considerably increases with the structural quality of material.

4.3. FT-Raman spectrum

The FT-Raman spectrum was measured with a Bruker FT-Raman spectrometer (Type FRA 106/IFS

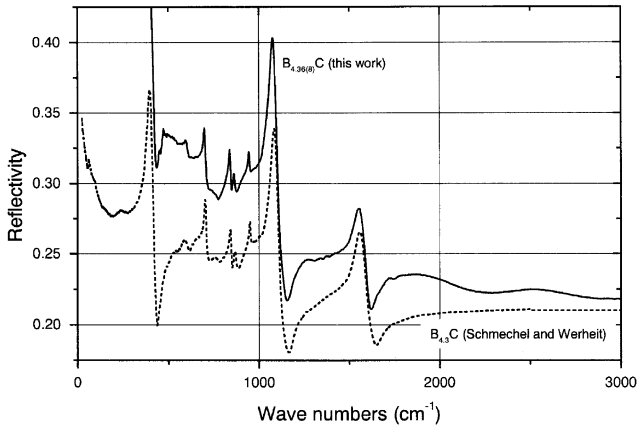

Fig. 3. IR-reflectivity spectrum of a $B_{4.36(8)}C$ single crystal compared with the spectrum of polycrystalline $B_{4.3}C$ [3].

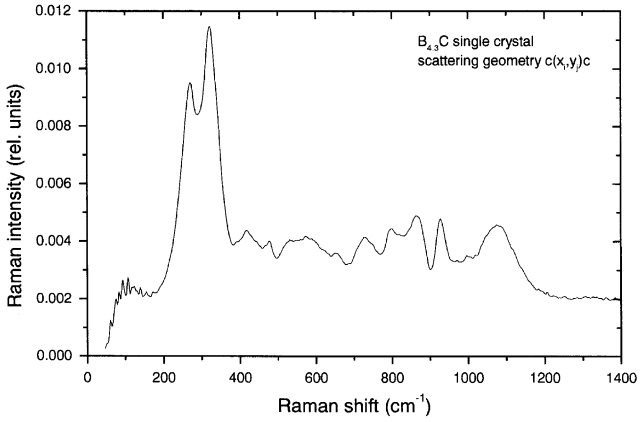

Fig. 4. Raman spectrum of a $B_{4.36(8)}C$ single crystal. The sample was cut perpendicular to the crystallographic c-axis. Scattering geometry $c(x_iy_j)c$. Resolution 2 cm^{-1}.

66v). To reduce noise, 6000 scanned interferograms were averaged and then Fourier-transformed into the real spectrum (Fig. 4). The Raman bands were analyzed by single or multiple Lorentzian fits; the peak frequencies are listed in Table 2. The weak noise of the spectrum allows to determine even weak Raman bands. The results are compared with results obtained on coarse crystalline $B_{4.3}C$ accordingly orientated by chance [17], with the Raman frequencies of $^{11}B_{4.3}C$ [18] and with theoretical calculations [19,20]. The agreement is satisfactory, though the present results are the most accurate ones for $B_{4.3}C$ with the natural isotope enrichment $^{10}B/^{11}B = 18.83/81.17$. For a detailed interpretation of the Raman bands, see Ref. [18].

There seems to be a weak band at 114(4) cm^{-1}, which could be attributed to the theoretically expected rotation mode of the icosahedra [19,20]. However, because of the influence of the Rayleigh-filter cutting the spectrum at 100 cm^{-1} and possibly slightly reducing the signal intensity in the adhered spectral range as well, it cannot be excluded that this band is simulated only.

5. Knoop hardness

It is well known that boron carbide is one of the hardest technical ceramics. However, the quantitative data of Vickers and Knoop hardness reported in literature spread over a wide range (see Refs. [1,21,22]). To allow a reliable comparison with carefully and systematically measured data like those reported in Ref. [21], the hardness measurements on our single crystal $B_{\sim 4.3}C$ were performed in the same laboratory (Wacker Ceramics, Kempten) and with the same equipment (Duriment, Leitz, Wetzlar). The averaged results of 10 measurements, each, are

HK 0.1 (load 1 N) of $B_{4.3}C$ single crystal (surface $\perp$c) : 36.7(6) GPa,

HK 0.1 (load 1 N) of $B_{4.3}C$ single crystal (surface $\parallel$c) : 33.8(7) GPa.

These values considerably exceed the hardness HK 0.1 = 29.70(15) GPa [21] of boron carbide with the nominal composition $B_{4.1}C$ by 14% and 24%, respectively. For both crystallographic orientations, this difference is above the margins of error by far. The reference boron carbide $B_{4.1}C$ really corresponds to $B_{4.3}C$, the composition at the carbon-rich limit of the homogeneity range, and contains a small amount of graphitic free carbon (see Refs. [1,23]). Obviously, the high value of the hardness of the single crystals is related to their high degree of perfection.

6. Conclusion

Significant properties of the high-quality single crystals compared with polycrystalline or hot-pressed boron carbide are the hardness, which is considerably higher, and the high optical absorption at energies below the absorption edge. Taking the IR-reflectivity spectrum into account as well, the dynamical electrical conductivity of the high-quality single crystals is proved to be considerably higher than that of lower-quality boron carbide. Taking the DC data into account, this seems to be caused by higher carrier mobility. The better resolution and lower noise level of the Raman spectrum allows to recognize some more weak Raman modes. Absorption bands below the absorption edge can be easily attributed to electronic transitions between levels in the band gap of the preliminary band scheme.

Table 2
Raman frequencies of a $B_{4.36(8)}C$ single crystal obtained with the scattering geometry $c(x_i, y_j)c$; compared with other experimental and theoretical results

	This work	Kuhlmann [17]	Exp. symm. type [17]	$^{11}B_{4.3}C$ [18]	Calc. frequencies [19,20]	Theor. symm. type [19,20]	Movement of structure elements [12,17,19]
1	(114(4))				172	E_g	Rotating icosahedron
2	266.6(4)	270	A_{1g}	267(1)			Rotating CBC chain and wagging ico.
3	323.5(3)	320	A_{1g}	319(1)	335	E_g	Rotating CBB chain and wagging icos
4	389(2)						
5	418(1)	420	A_{1g}	414(2)			
6	445(2)	449	E_g				
7	477(1)	477	E_g	477(2)			
8	529(1)	532	E_g	526(3)	546/51	A_{1g}/E_g	No chain
9	573(5)	560	E_g?	566(3)	589	A_{1g}	
10	603(8)	591	E_g?				
11	654(1)	652	E_g	646(3)	655	E_g	
12	724(2)	725	E_g	720(2)	692	E_g	
13	747(5)						
14	797(2)	797	A_{1g}	790(2)	828	A_{1g}	
15	831(4)						
16	860(2)	869	A_{1g}	862(2)			
17	875(2)						
18	929(1)	928	A_{1g}	923(2)	964	A_{1g}	Symmetrically stretching chain
		990			1004	E_g	
					1016	E_g	Rotating chain and stretching icos
19	1044(5)	1065	A_{1g}	1040(3)			Breathing B_{12} icosahedron
20	1085(2)			1078(2)	1078	A_{1g}	Breathing $B_{11}C$ icosahedron

References

[1] H. Werheit, Boron compounds, in: O. Madelung (Ed.), Landolt–Börnstein, Numerical Data and Functional Relationships in Science and Technology, New Series Group III, Vol. 41D, Springer, Berlin, 2000, pp. 1–491.
[2] R. Schmechel, H. Werheit, J. Solid State Chem. 154 (2000) 61.
[3] R. Schmechel, H. Werheit, J. Phys.: Condens. Matter 11 (1999) 6803.
[4] H. Werheit, T. Au, R. Schmechel, S.O. Shalamberidze, G.I. Kalandadze, A.M. Erstavi, J. Solid State Chem. 154 (2000) 79.
[5] A. Leithe-Jasper, T. Tanaka, 13th International Symposium on Boron, Borides and Related Compounds, Dinard, France, September 5–10, 1999, contribution O 22.
[6] R. Falckenberg, Thesis, Technische Hochschule, München, Germany, 1965.
[7] R. Emeis, Z. Naturforschg. 9a (1954) 67.
[8] T. Tanaka, S. Otani, Y. Ishizawa, J. Crystal Growth 73 (1985) 31.
[9] T. Tanaka, Z. Urek, Joe Wong, M. Rowen, J. Crystal Growth 192 (1998) 141.
[10] W. Borchert, E. Born, Kristall. Techn. 4 (1969) 293.
[11] I.D.R. Mckinnon, T.A. Aselage, S.B. Van Deusen, AIP Conf. Proc. 140 (1986) 114.
[12] H. Werheit, H. Binnenbruck, A. Hausen, Phys. Stat. Sol. (b) 47 (1971) 153.
[13] H.L. Tardy, T.L. Aselage, D. Emin, AIP Conf. Proc. 231 (1991) 138.
[14] H. Werheit, M. Laux, U. Kuhlmann, R. Telle, Phys. Stat. Sol. (b) 172 (1992) K.
[15] R. Schmechel, Thesis, Gerhard Mercator University, Duisburg, Germany, 1998.
[16] R. Schmechel, H. Werheit, J. Mater. Process. Manuf. Sci. 6 (1998) 329.
[17] U. Kuhlmann, H. Werheit, Phys. Stat. Sol. (b) 175 (1993) 85.
[18] H. Werheit, H.W. Rotter, F.D. Meyer, H. Hillebrecht, S.O. Shalamberidze, T.G. Abzianidze, G.G. Esadze, J. Solid State Chem.
[19] K. Shirai, S. Emura, J. Phys.: Condens. Matter 8 (1996) 10919.
[20] K. Shirai, S. Emura, J. Solid State Chem. 133 (1997) 93.
[21] A. Lipp, K. Schwetz, Ber. Dt. Keram. Ges. 52 (1975) 335.
[22] H. Werheit, Boron compounds, in: O. Madelung (Ed.), Landolt–Börnstein, Numerical Data and Functional Relationships in Science and Technology, New Series, Group III, Vol. 17g, Springer, Berlin, 1984, pp. 1–62.
[23] K.A. Schwetz, P. Karduck, AIP Conf. Proc. 231 (1991) 405.